Degradation-induced energy level mismatch in cohost-dopant blue phosphorescent OLEDs after device operation

Kiwoong Kim,[a] Won Jae Chung,[b] Junseop Lim,[b] Kyu-Joon Lee,[c] Hong-Hee Kim,[d] Thorsten Schultz,[e] Patrick Amsalem,[f] Won-Kook Choi,[d] Hong-Kyu Kim,[c] Jae-Pyoung Ahn,[c] Hyunbok Lee,[g] Jun Yeob Lee,[b,*] Soohyung Park[c,*] and Yeonjin Yi[a,*]

[a]*Department of Physics and van der Waals Materials Research Center, Yonsei University, 50 Yonsei-ro, Seodaemun-gu, Seoul 03722, Republic of Korea*

[b]*School of Chemical Engineering, Sungkyunkwan University, 2066 Seobu-ro, Jangan-gu, Suwon-si, Gyeonggi-do 16419, Republic of Korea*

[c]*Advanced Analysis Center, Korea Institute of Science and Technology, 5 Hwarang-ro 14-gil, Seongbuk-gu, Seoul, 02792, Republic of Korea*

[d]*Center of Opto-Electronic Materials and Devices, Post-Silicon Semiconductor Institute, Korea Institute of Science and Technology, 5 Hwarang-ro 14-gil, Seongbuk-gu, Seoul 02792, Republic of Korea*

[e]*Helmholtz-Zentrum für Materialien und Energie GmbH, Bereich Solarenergieforschung, Albert-Einstein Straße 15, 12489 Berlin, Germany*

[f]*Institut für Physik & IRIS Adelershof, Humboldt-Universität zu Berlin, Brook-Taylor Straße 6, 12489 Berlin, Germany*

[g]*Department of Physics, Kangwon National University, 1 Gangwondaehak-gil, Chuncheon-si, Gangwon-do, 24341, Republic of Korea*

*Corresponding authors.

E-mail addresses: leej17@skku.edu; soohyung.park@kist.re.kr; yeonjin@yonsei.ac.kr

ABSTRACT

Phosphorescent organic light-emitting diodes (PhOLEDs) have been considered potential candidates for high-efficiency blue emission. However, their short lifetime has been an issue, and much effort has been put into resolving this. Among such efforts, understanding energy level alignments (ELA) is one of the essential factors in understanding the degradation. However, ELA inside the actual PhOLED is rarely studied due to technical limitations. Here, we comprehensively investigate the degradation mechanism of blue PhOLEDs consisting of a cohost-dopant type emissive layer (EML). The blue PhOLEDs are aged with typical operating conditions until the luminance performance degrades. Ultraviolet and X-ray photoelectron spectroscopy (UPS and XPS) combined with a damage-free gas cluster ion beam (GCIB) etching and transmission electron microscopy-energy dispersive X-ray spectroscopy (TEM-EDX) unveil the buried interfaces inside the PhOLEDs. XPS and TEM-EDX measurements show that the dopant is unlikely to be the primary origin of the device degradation. Instead, UPS measurements show that the ELAs at the interfaces facing the EML are significantly altered unfavorably after device aging. This implies that the changes in the ELA are the leading cause of PhOLED degradation. Our results highlight the importance of retaining the ELAs during device operation to achieve long-lifetime blue PhOLEDs.

Keywords: Blue phosphorescent OLEDs; Cohost-dopant system; Energy level alignment; Degradation; Aging; Molecular aggregation; FIrpic; UPS; XPS; GCIB; Depth profile

1. Introduction

Organic light-emitting diodes (OLEDs) have attracted much attention in the display research community due to their high color purity, high contrast, and high efficiency. In particular, phosphorescent OLEDs (PhOLEDs) have been successfully commercialized by achieving an internal quantum efficiency close to 100%, beyond the intrinsic limit of fluorescent emission [1–8]. Recently, a cohost-dopant system in the emissive layer (EML) has been suggested to achieve highly efficient PhOLEDs. In cohost-dopant PhOLEDs, holes and electrons transported to the cohost generate exciplex states, then they transfer energy to dopants, and finally, the dopants emit light. This cohost-dopant system significantly maximizes external quantum efficiency (EQE) [6–14].

Despite the remarkably high EQE of the cohost-dopant PhOLEDs, their short lifetime is still an open problem. So far, many studies have focused on molecule dissociation as a culprit for the short lifetime with various experimental approaches [15–22]. These studies report that the bond breaking of blue dopants (*e.g.*, bis[2-(4,6-difluorophenyl)pyridinato-C2,*N*](picolinato)iridium(III), FIrpic) and their J-type aggregation are the leading causes for the degradation of blue PhOLEDs [15–17,23–25]. Mass spectroscopy, liquid chromatography, and matrix-assisted laser desorption/ionization measurements have been employed to determine the fragmentation route of the blue dopants [16–18,23,26]. For example, the chemical bonds between the Ir atom and the picolinate ligands in FIrpic break upon aging [16,17,23,24]. It has been reported that the long exciton lifetime of phosphorescence is the driving force for bond breakage, which increases the bi-molecular processes reducing the molecular stability [15,25,27,28].

Another critical property determining device performance is the energy level alignment (ELA) at each interface inside PhOLEDs. For efficient PhOLEDs, the energy levels of organic materials must be appropriately aligned at each interface inside the device. However, the

deterioration of the ELA after device operation is rarely studied, limiting comprehensive understanding of the PhOLED degradation. This is because there has been no experimental method to measure the ELA inside the actual device after operation. For this reason, previous results have been obtained by mimicking the degradation of actual PhOLEDs using single-layer films or solutions [16–22]. In other approach, they reconstructed the device structure step-by-step using the bilayer consisting of two single neat films [29]. However, such indirect approaches cannot resolve information on the interlayer charge transfer and interlayer molecular diffusion/aggregation. In order to overcome such limitations, recent studies have emphasized that individual PhOLEDs themselves should be studied directly, not using single-layer films or solutions. To this end, ultraviolet/X-ray photoelectron spectroscopy (UPS/XPS) depth profile analyses with damage-free Ar gas cluster ion beams (GCIB) have been recently suggested [30,31]. GCIB enables surface etching by clusters of a few thousand Ar atoms without damaging the underlying layer because the energy-per-atom of Ar GCIB is approximately three orders of magnitude lower (a few eV) than that of a conventional Ar^+ ion sputtering beam (a few keV). Consequently, GCIB enables probing of the intrinsic layer-by-layer properties inside the actual PhOLEDs.

In this study, we report ELA changes by degradation using UPS and XPS combined with the GCIB etching technique. As cohost-dopant PhOLEDs, we fabricated blue PhOLEDs in which the EML consists of an exciplex cohost, *N,N´*-dicarbazolyl-3,5-benzene (mCP) and (1,3,5-triazine-2,4,6-triyl)tris-(benzene-3,1-diyl))tris(diphenylphosphine oxide) (PO-T2T), doped with a FIrpic blue emitter. The degradation of blue PhOLEDs with and without blue dopants is compared to understand the role of dopants in degradation, where they have been considered a leading cause of degradation [15–17,23–25]. Transmission electron microscopy-energy dispersive X-ray spectroscopy (TEM-EDX) analysis was also conducted to observe the molecular diffusion after device aging.

2. Experimental

2.1 Device Fabrication

Indium tin oxide (ITO) substrates were cleaned by sequential ultrasonication with acetone, deionized water, and isopropyl alcohol for 10 min each, followed by UV-ozone treatment to remove residual contaminants on the ITO surface. Then, poly(3,4-ethylenedioxythiophene):poly(styrene sulfonate) (PEDOT:PSS) was spin-coated onto the cleaned ITO substrates at a rate of 500 rpm for 5 s and 1000 rpm for 45 s. Samples were then loaded into the entry chamber and transferred to the deposition chamber at a base pressure of 4.0×10^{-7} Torr. The organic layers and cathode were thermally evaporated sequentially, and the deposition thickness was estimated via a calibrated quartz thickness monitor. As the hole transport layer (HTL) and the electron blocking layer, 4,4′-cyclohexylidenebis[*N,N*-bis(4-methylphenyl)aniline (TAPC) and mCP were deposited with rates of 1 Å s^{-1} and 0.5 Å s^{-1}, respectively. For fabricating the cohost-dopant EML, mCP, PO-T2T, and FIrpic were co-deposited with rates of 0.45 Å s^{-1}, 0.45 Å s^{-1}, and 0.1 Å s^{-1}. Diphenylphosphine oxide-4-(triphenylsilyl)phenyl (TSPO1) and 2,2′,2″-(1,3,5-benzinetriyl)-tris(1-phenyl-1-H-benzimidazole) (TPBi) were deposited as the hole blocking and the electron transport layer (ETL) with rates of 0.5 Å s^{-1} and 1 Å s^{-1}. Finally, LiF and Al were sequentially deposited at rates of 0.1 Å s^{-1} and 5 Å s^{-1} as the electron injection layer and cathode. The final structure (Fig. 1a) of the blue PhOLEDs is ITO (150 nm)/PEDOT:PSS (40 nm)/TAPC (10 nm)/mCP (10 nm)/mCP:PO-T2T:FIrpic (25 nm, 0.45:0.45:0.1 in wt%)/TSPO1 (5 nm)/TPBi (20 nm)/LiF (1.5 nm)/Al (200 nm). The PhOLEDs without FIrpic were fabricated in the same way. The current density-voltage-luminance (*J–V–L*) characteristics of PhOLEDs were measured using a Keithley 2400 source-measure unit (Tektronix Inc.) combined with a Konica Minolta CS-2000 spectroradiometer.

2.2 UPS, IPES, and XPS measurements

UPS and XPS measurements were performed using a hemispherical energy analyzer (Nexsa, Thermo Scientific Inc.) with He Iα ultraviolet ($h\nu$ = 21.22 eV) and Al Kα X-ray ($h\nu$ = 1486.6 eV) light sources. An Ar GCIB source (MAGCIS, Thermo Scientific Inc.) was used for sequential etching for the organic layers. Inverse photoelectron spectroscopy (IPES) measurements were performed in isochromat mode with a low-energy electron gun and a bandpass filter (SrF_2–NaCl combination for 9.5 eV pass energy). The energy reference of UPS, IPES, and XPS was calibrated using clean Au. The encapsulated PhOLEDs were loaded into the Ar-filled glove box, and then the top LiF/Al layers were peeled off after removing the cover glass to exclude any possible degradation by environmental exposure [32,33]. The samples were then transferred from the glove box to the analysis chamber without breaking the Ar atmosphere. The base pressure of the analysis chamber was maintained at 1.0×10^{-10} Torr. During the LiF/Al peel-off process, the underlying TPBi layer can be damaged by the residual LiF and mechanical stress. Thus, the TPBi layer was removed by GCIB etching before the depth profile measurements and was not considered for the interface analysis.

2.3 Optimization and calibration of GCIB etching

The reliability of GCIB etching was tested by changing the Ar-cluster sizes in the range of 1,000 ~ 4,000 atoms and the acceleration voltages in the range of 2 ~ 4 keV. The optimized Ar-clusters size and acceleration voltage for damage-free etching were 1000 Ar atoms and 2.0 keV for our instrumental setup. With such conditions, we obtained reliable etching results for conserving pristine layer properties (Fig. S1). This condition is comparable with previous studies [30,31]. The GCIB etching rate was calibrated from the total thickness of PhOLEDs determined by TEM with the total etching time. The average etching rate of GCIB was *ca*. 2.5 nm min^{-1}, and the etching time between depth profile measurements was set at 1 min.

2.4 TEM-EDX measurements

TEM-EDX measurements were conducted to explore the molecular distribution of pristine and aged PhOLEDs. Cross-section samples were prepared using a focused ion beam milling technique (FIB; Helios NanoLab 600, FEI), and TEM images were obtained with Talos F200X (FEI) equipped with four windowless Si drift detectors. The EDX signals were collected at an accelerating voltage of 200 kV (Schottky X-FEG gun) for 10 min corresponding to 3.5 ms $pixel^{-1}$ dwell time, which is sufficient to guarantee a high signal-to-noise ratio.

3. Results and discussion

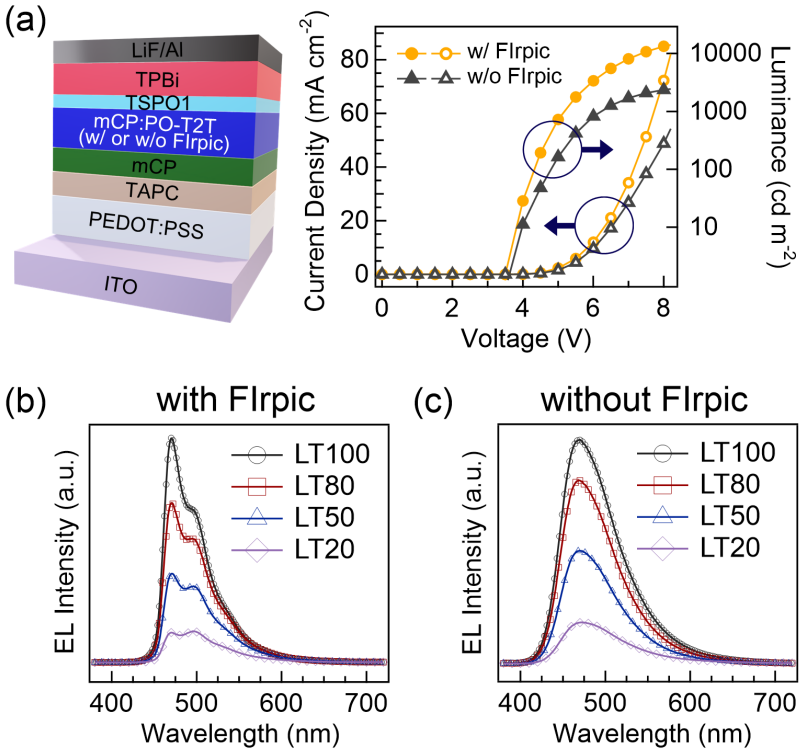

Fig. 1. (a) Device structure and *J*–*V*–*L* characteristics of PhOLEDs with and without FIrpic. EL spectra of LT100, LT80, LT50, and LT20 with (b) and without (c) FIrpic at a bias of 5 V. (See the text for the definition of LT100, LT80, LT50, and LT20).

The blue PhOLEDs were fabricated with and without the FIrpic dopant to understand the role of the dopant in the degradation process. Fig. 1a shows the PhOLED structure and the *J*–*V*–*L* characteristics. The PhOLED with FIrpic shows much better *J*–*V*–*L* characteristics, resulting in a higher EQE of 16.7 % than without FIrpic of 7.6 % (Fig. S2). This implies that the FIrpic dopant significantly improves blue emission efficiency. Figs. 1b and 1c show the electroluminance (EL) spectra of PhOLEDs with and without FIrpic according to the degree of degradation. The PhOLED showing an initial EL intensity of 1000 cd m^{-2} is denoted as LT100. After continuous operation upon constant-current aging, the EL intensity of the PhOLED decreases to 80 %, 50 %, and 20 % from its initial EL intensity. These degraded PhOLEDs are denoted as LT80, LT50, and LT20. Comparing the EL spectra of PhOLEDs with (Fig. 1b) and

without (Fig. 1c) FIrpic, the spectral shapes are different due to their different light emission processes (the mCP:PO-T2T cohost exciplex predominates emission spectra without FIrpic whereas phosphorescent emission occurs by energy transfer from the cohost exciplex to the FIrpic dopant with FIrpic, see Fig. S3). However, both PhOLEDs show a similar degradation tendency regardless of the FIrpic doping, as shown in Figs. 1b and 1c. Notably, the EL intensity gradually decreases with a similar rate in both PhOLEDs. Thus, FIrpic dopants are unlikely to be the leading cause for the EL decrease in our PhOLEDs, showing discrepancies from previous reports [15–17,23–25]. To find the origin of EL reduction, we first investigated each molecule's chemical state changes inside PhOLEDs via XPS depth profile measurements.

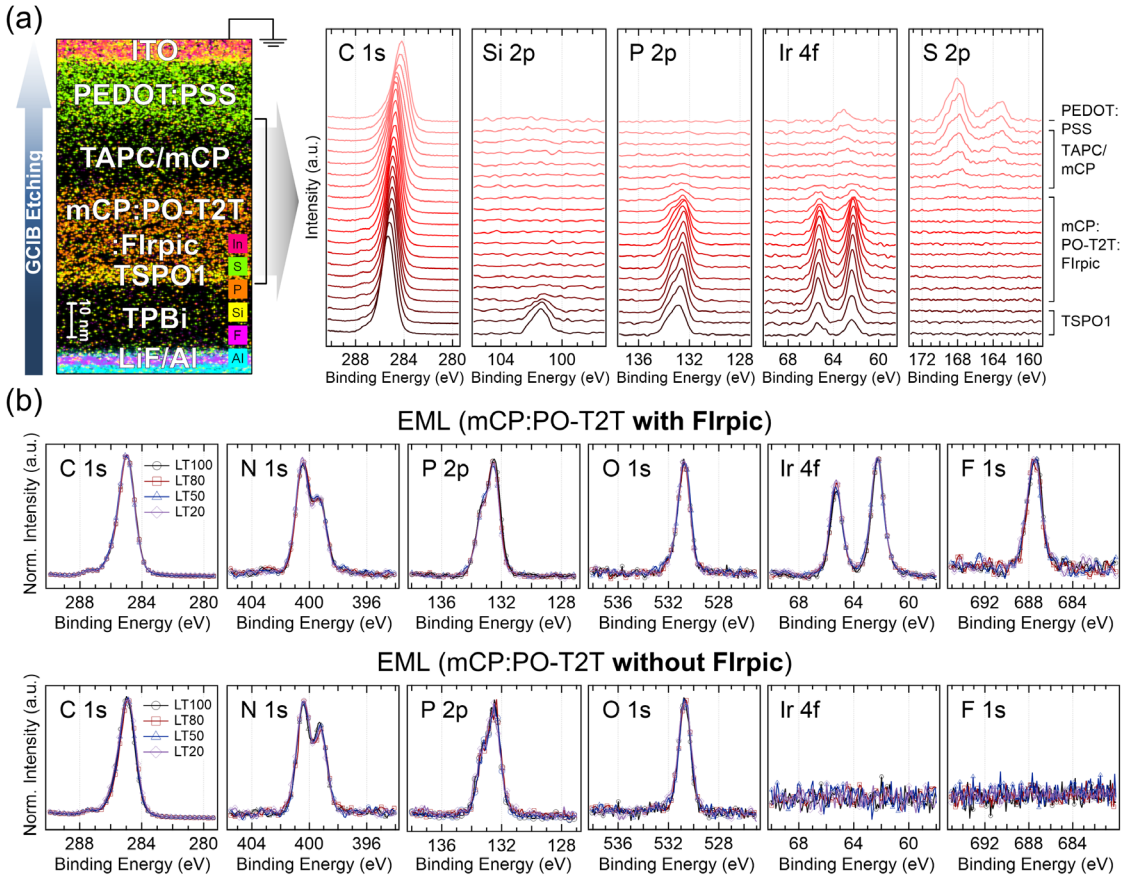

Fig. 2. (a) TEM-EDX cross-sectional image showing different elements for each layer of the PhOLED and corresponding XPS depth profiles of the LT100 with FIrpic. (b) Normalized XPS core level spectra of the EML for LT100, LT80, LT50, and LT20 (EL intensity of the PhOLED decreases to 80 %, 50 %, and 20 % from its initial EL intensity by device degradation) with

and without FIrpic. (Similar comparisons for other layers are presented in Figs. S5 and S6).

Fig. 2 shows the XPS depth profile measurements with GCIB from the TSPO1 ETL to the ITO anode for pristine and degraded PhOLEDs. The cross-sectional TEM-EDX analysis confirms a well-defined multilayer structure, and corresponding XPS depth profiles are shown in Fig. 2a. The evolution of the exclusive elemental peak for each layer (Si 2p for TSPO1, P 2p for TSPO1 and PO-T2T, Ir 4f for FIrpic, and S 2p for PEDOT:PSS, Fig. S4 for chemical structures of each molecule) indicates successful GCIB etching. (Small features in Ir 4f panel at PEDOT:PSS region correspond to Na-based impurities from PEDOT:PSS.)

In Fig. 2b, the normalized XPS core-level spectra of the EML are shown to thoroughly observe possible chemical state changes of FIrpic or the cohost. Remarkably, none of the XPS core-level spectra shows any chemical state change signal, and the core-level spectra remain virtually identical from LT100 to LT20. Furthermore, the other layers also do not show significant changes in XPS core-levels (Figs. S5 and S6). Although a tiny amount of molecular bond changes below the XPS detection limit (approximately 0.1 %) cannot be completely ruled out, most molecules inside the device, including FIrpic, are chemically robust enough to resist the aging process. This suggests another mechanism is causing the EL performance deterioration observed in Fig. 1; *e.g.*, molecular diffusion and aggregation are one of the well-known origins of EL reduction [19,25,34,35]. Therefore, we investigated the molecular diffusion/aggregation by device operation via TEM-EDX elemental mapping..

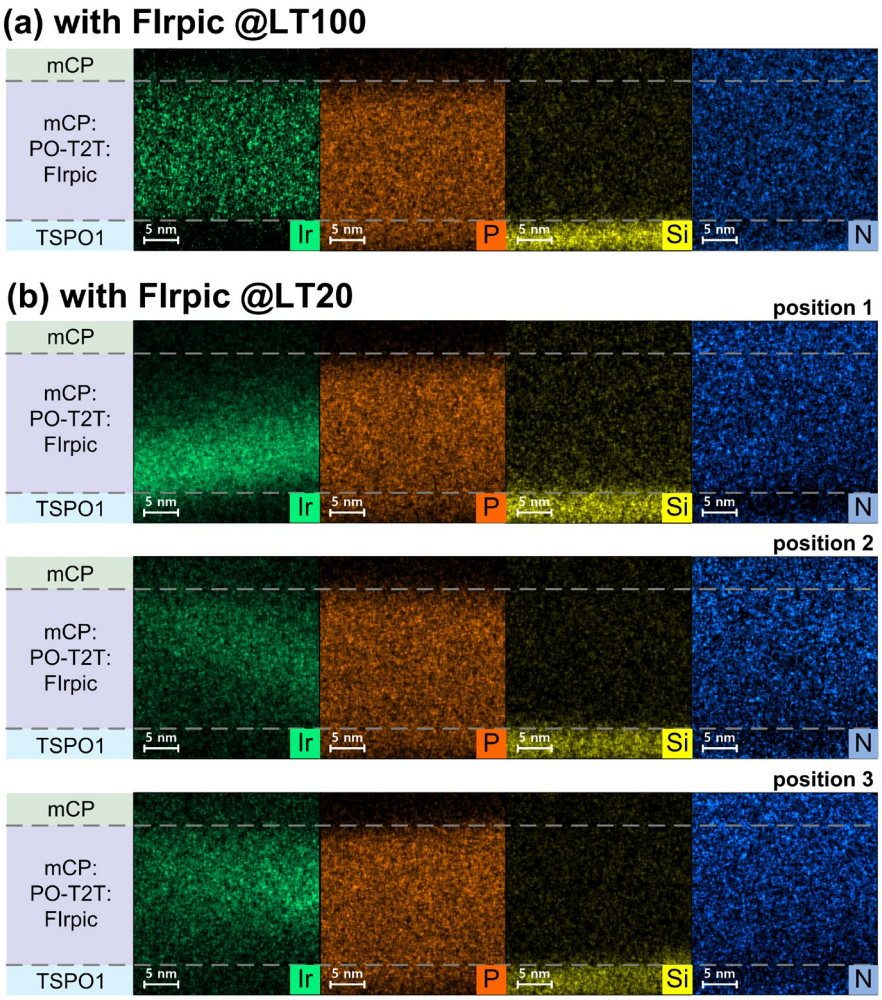

Fig. 3. TEM-EDX elemental maps at the interface of ETL (TSPO1)/EML (mCP:PO-T2T: FIrpic)/HTL (mCP). Ir (FIrpic), P (PO-T2T), and Si (TSPO1) map for LT100 (a) and LT20 (b). Three different positions were analyzed for LT20 (b) to confirm the diffusion reliably.

Fig. 3 shows TEM-EDX elemental maps for the EML and adjacent layers in LT100 and LT20. The elemental maps for LT20 were measured at three different positions to see the diffusion reliably. The TSPO1 (ETL)/EML interface in Figs. 3a and 3b is distinguished clearly by the Si atoms in the TSPO1 layer (yellow region). This suggests that the interfacial molecular diffusion/mixing between TSPO1 and EML is negligible under the experimental detection limit (approximately 1 %). Ir and P clearly identify the FIrpic and PO-T2T in the EML in Fig. 3a; the LT100 shows a uniform FIrpic and PO-T2T distribution. However, LT20 (Fig. 3b) shows a significant molecular aggregation of FIrpic in the EML while PO-T2T is still uniform. Wang

et al. reported that the J-type aggregation of FIrpic leads to broader emission in the EL spectra [25], which is also observed in the EL peak (Fig. S7). The applied electric field was suggested as the driving force for the FIrpic aggregation. However, in Fig. 3b, although the electric field is applied to the vertical direction, FIrpic does not aggregate directionally but rather randomly at various positions. This indicates that the electric field cannot be the sole cause for the aggregation. We propose additional thermal diffusion assisted by Joule heating during device operation as another possible driving force for the observed aggregation [36–38].

This dopant (emitter) aggregation would deteriorate the EL efficiency in two ways. The first is the emission zone reduction due to the emitter aggregation observed in Fig. 3. The other and more fundamental aspect is that the dopant aggregation would lead to a new Fermi level (E_F) equilibrium, which modifies the ELA near the EML. Therefore, we measured the ELA at each interface inside the PhOLEDs before and after device operation..

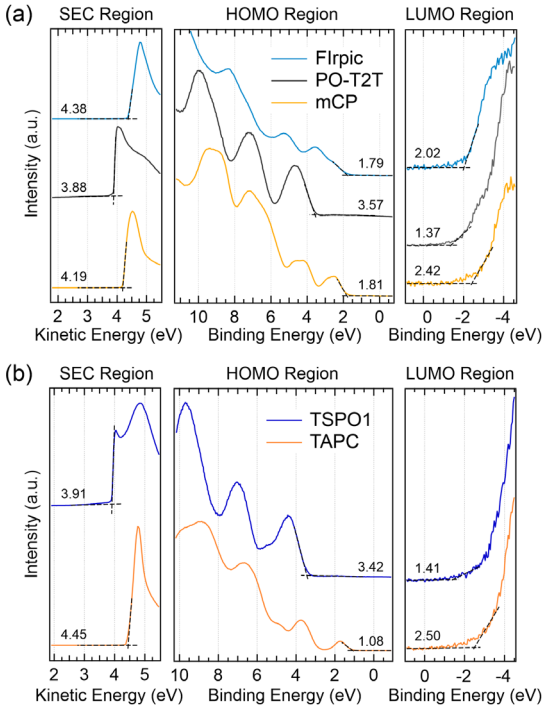

Fig. 4. UPS and IPES spectra of neat films of (a) mCP, PO-T2T, and FIrpic and (b) TSPO1, and TAPC.

Prior to measure the ELA inside PhOLED device, we measured the single neat films as a reference as shown in Fig. 4. The work function (WF) of single neat films are determined by the onset of the secondary elecctron cutoff spectra. The highest occupied molecular orbital (HOMO) and lowest unoccupied molecular orbital (LUMO) of single neat films are evaluated by onset of UPS and IPES spectra, respectively. The ionization energy (WF + HOMO), electron affinities (WF – LUMO), and transport bandgap (HOMO + LUMO) of each neat films are summrized in Table 1.

Table 1. The ionization energy (IE), electron affinities (EA), transport bandgap (E_g) of mCP, PO-T2T, FIrpic, TSPO1, and TAPC.

	mCP	**PO-T2T**	**FIrpic**	**TSPO1**	**TAPC**
IE	6.00 eV	7.45 eV	6.17 eV	7.33 eV	5.53 eV
EA	1.77 eV	2.51 eV	2.36 eV	2.50 eV	1.95 eV
E_g	4.23 eV	4.94 eV	3.81 eV	4.83 eV	3.58 eV

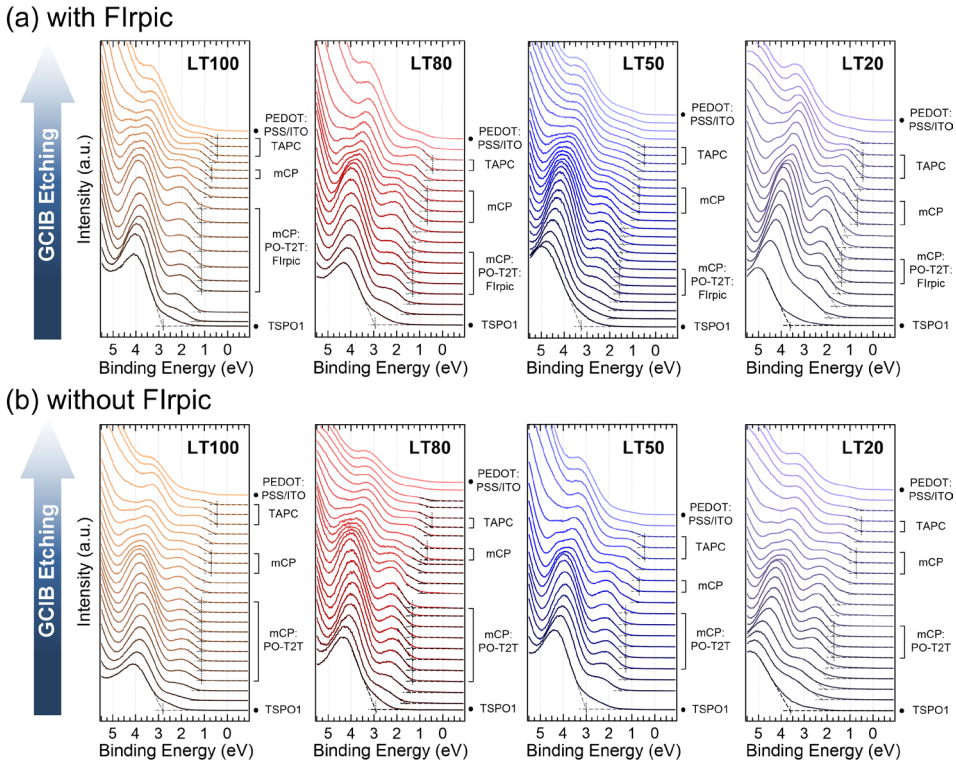

Fig. 5. UPS depth profiles for the HOMO region of PhOLEDs for LT100, LT80, LT50, and LT20 (a) with and (b) without FIrpic. The HOMO onset of each layer was cross-checked from single neat molecular films (Fig. 4).

Fig. 5 shows the UPS depth profiles for the full PhOLEDs with and without the FIrpic dopant according to the degree of degradation. With the information about neat films, each spectrum in Fig. 5 was identified by comparing it with the above spectrum. For all panels in Fig. 5, the spectral features gradually evolve from TSPO1 to PEDOT:PSS, indicating well-defined layer structures. Both PhOLEDs in Figs. 5a and 5b show quite similar spectral evolution across each layer for all degradation stages (LT100 ~ LT20) regardless of FIrpic doping. For quantitative analysis, HOMO onset of each spectrum was evaluated, shown as dashed lines in Fig. 5. Unlike the other layers, the EML has a composite structure consisting of mCP, PO-T2T, and FIrpic. Thus, the onsets of individual HOMO were estimated with the peak deconvolution process (Fig. S8). The LUMO level of each layer was estimated from the energy difference between transport bandgap and estimated HOMO level. With these evaluated onset

values, we obtained the ELA at the interfaces inside the whole PhOLEDs, as shown below.

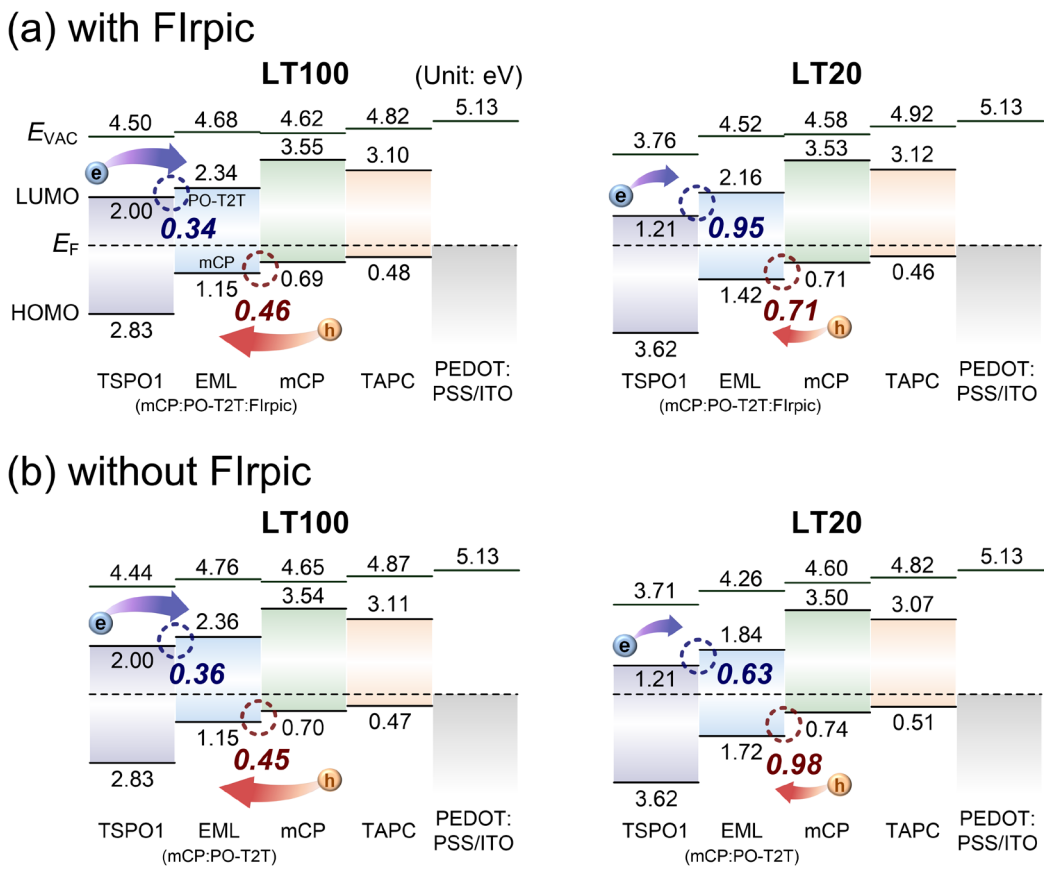

Fig. 6. Energy level diagrams for LT100 and LT20 in blue PhOLEDs with (a) and without (b) FIrpic. The energy level positions are indicated with respect to the E_F, and the dashed circles show the electron (blue) and hole (red) injection barriers at EML interfaces. The transport levels in the EML are evaluated from the cohost levels, *i.e.*, HOMO of mCP and LUMO of PO-T2T.

The ELA at each interface obtained from the UPS depth profiles is presented in Fig. 6. Here, the hole and electron transport levels in the EML are evaluated from the deconvoluted cohost level, *i.e.*, HOMO of mCP and LUMO of PO-T2T. To clarify the effect of dopant on the ELA, LT100 and LT20 were compared with and without FIrpic dopant, respectively.

The ELA at all interfaces for LT100 in Figs. 6a and 6b is nearly identical regardless of the FIrpic doping. This indicates that the FIrpic doping does not essentially influence the ELA within PhOLEDs before the degradation. On average, the electron injection barrier (Φ_e) of 0.35

eV from TSPO1 to EML and the hole injection barrier (Φ_h) of 0.46 eV from mCP to EML, 0.22 eV from TAPC to mCP, and 0.48 eV from PEDOT:PSS to TAPC are induced in both LT100 with and without FIrpic. For the extreme LT20 degradation, significant changes are observed from the initial LT100. In Fig. 6a, Φ_e at the TSPO1/EML interface increases from 0.34 to 0.95 eV. Φ_h at the EML/mCP, mCP/TAPC, and TAPC/PEDOT:PSS interfaces changes from 0.46 to 0.71 eV, from 0.21 to 0.25 eV, and from 0.48 to 0.46 eV, showing that Φ_h are essentially unchanged except at the EML/mCP interface. Even in the absence of FIrpic, the changes are similar to the case with Firpic. That is, in Fig. 6b, Φ_e at the TSPO1/EML interface changes from 0.36 to 0.63 eV. Φ_h at the EML/mCP, mCP/TAPC, and TAPC/PEDOT:PSS interfaces increases from 0.45 to 0.98 eV, from 0.23 to 0.23 eV (unchanged) and from 0.47 to 0.51 eV, showing that Φ_h is also essentially unchanged except at the EML/mCP interface.

The trend of energy level changes is nearly identical for both PhOLEDs with and without the FIrpic dopant. This is also consistent with the lifetime characteristics (Fig. S9). As seen in Figs. 6a and 6b, both the TSPO1 and EML energy levels are lowered after the LT20 aging, but the TSPO1 lowering is much larger than EML. In contrast, mCP, TAPC, and PEDOT:PSS in the HTL side are nearly intact after the LT20 aging. These asymmetric lowerings in different layers result in substantial increases in barriers at the EML interfaces. These barrier increases accord well with the reduced *J-V-L* and EQE characteristics (Fig. S10, S11, and Table S1). We speculate that the rise of Φ_e and Φ_h would originate from the exciplex/emitter irradiation and electrical/thermal stress near the EML interfaces over the molecular aggregation observed. This stress could form an interface state inducing interlayer charge transfer, particularly near the EML. This interlayer charge transfer can pin the E_F away from its original position. In consequence, the presence of such stress-induced interface state can alter the ELA at the interface [39–41]. It is very consistent with the previous understanding suggested by Yang et al. and Fahlman. They reported this interlayer charge transfer hinder the forming the simple vacuum level alignment,

resulting in the re-alignment of interface energy level. [42-44]. Further, it is reported that the changes in ELA signficanrtly impact on the electrical properties of devices [45].

We can summarize our observations: (1) FIrpic is not directly involved in the EL degradation process within the detection limit of the current analysis. It only shows broader and reduced EL emissions driven by diffusion/aggregation. (2) the aging-induced energy level mismatch to the adjacent layers to the EML is crucial for the degradation. We propose that this energy level mismatch stems from stress-induced interface state at the EML interface. Our results strongly suggest that focusing on the origins of ELA changes at heterointerfaces is essential for understanding the EL degradation process and ultimately overcoming the short lifetime of PhOLEDs.

4. Conclusion

We investigated the degradation of PhOLEDs consisting of the cohost-dopant type EML. The PhOLEDs were aged with typical device operating conditions until the device performance decreased to 80, 50, and 20 % of the initial EL intensity. Before and after the degradation, XPS and UPS depth profile technique with GCIB revealed the changes in chemical bond and energy level alignment at each interface inside the PhOLEDs. XPS depth profiles suggest that most molecules remain intact in each layer of PhOLEDs within the detection limit. The FIrpic dopant is also stable enough upon device operation, and only molecular aggregation is observed. Most importantly, the energy level alignment at the interface facing the EML is changed significantly after device aging, regardless of the FIrpic doping. Thus, the dopant itself is not the dominant factor for the PhOLED degradation, but the degradation correlates with the changes in the energy level alignment after device operation. Our results emphasize the importance of retaining the optimized energy level alignment under device operation for achieving long-lifetime blue PhOLEDs.

CRediT authorship contribution statement

Kiwoong Kim: Conceptualization, Methodology, Validation, Formal analysis, Investigation, Writing – original draft. **Won Jae Chung:** Resources. **Junseop Lim:** Resources. **Kyu-Joon Lee:** Investigation. **Hong-Hee Kim:** Investigation. **Thorsten Schultz:** Investigation. **Patrick Amsalem:** Investigation. **Won-Kook Choi:** Investigation. **Hong-Kyu Kim:** Investigation. **Jae-Pyoung Ahn:** Investigation. **Hyunbok Lee:** Investigation, Writing – review & editing. **Jun Yeob Lee:** Supervision, Funding acquisition, Resources, Writing – review & editing. **Soohyung Park:** Supervision, Funding acquisition, Resources, Writing – review & editing. **Yeonjin Yi:** Supervision, Funding acquisition, Resources, Writing – review & editing.

Declaration of Competing Interest

The authors declare that they have no known competing financial interests or personal relationships that could have appeared to influence the work reported in this paper.

Acknowledgements

This work was supported by the National Research Foundation of Korea [NRF-2020R1A2C2014644, 2018M3D1A1058793, 2022M3D1A2083799, and 2017R1A5A1014862 (SRC program: vdWMRC center)], the Graduate School of YONSEI University Research Scholarship Grants, Samsung Display Company, KIST Institutional Program (Project No. 2V09352), and an Industry-Academy joint research program between Samsung Electronics and Yonsei University.

Appendix A. Supplementary material

References

[1] M. A. Baldo, D. F. O'Brien, Y. You, A. Shoustikov, S. Sibley, M. E. Thompson, S. R. Forrest, Highly efficient phosphorescent emission from organic electroluminescent devices, Nature. 395 (1998) 151-154. https://doi.org/10.1038/25954.

[2] C. Adachi, M.A. Baldo, M.E. Thompson, S.R. Forrest, Nearly 100% internal phosphorescence efficiency in an organic light emitting device, J. Appl. Phys. 90 (2001) 5048–5051. https://doi.org/10.1063/1.1409582.

[3] Y. Sun, N.C. Giebink, H. Kanno, B. Ma, M.E. Thompson, S.R. Forrest, Management of singlet and triplet excitons for efficient white organic light-emitting devices, Nature. 440 (2006) 908–912. https://doi.org/10.1038/nature04645.

[4] S.J. Su, E. Gonmori, H. Sasabe, J. Kido, Highly efficient organic blue-and white-light-emitting devices having a carrier- And exciton-confining structure for reduced efficiency roll-off, Adv. Mater. 20 (2008) 4189–4194. https://doi.org/10.1002/adma.200801375.

[5] S.-Y. Kim, W.-I. Jeong, C. Mayr, Y.-S. Park, K.-H. Kim, J.-H. Lee, C.-K. Moon, W. Brütting, J.-J. Kim, Organic Light-Emitting Diodes with 30% External Quantum Efficiency Based on a Horizontally Oriented Emitter, Adv. Funct. Mater. 23 (2013) 3896–3900. https://doi.org/10.1002/adfm.201300104.

[6] H. Shin, S. Lee, K.-H. Kim, C.-K. Moon, S.-J. Yoo, J.-H. Lee, J.-J. Kim, Blue Phosphorescent Organic Light-Emitting Diodes Using an Exciplex Forming Co-host with the External Quantum Efficiency of Theoretical Limit, Adv. Mater. 26 (2014) 4730–4734. https://doi.org/10.1002/adma.201400955.

[7] T. Xu, J.-G. Zhou, C.-C. Huang, L. Zhang, M.-K. Fung, I. Murtaza, H. Meng, L.-S. Liao, Highly Simplified Tandem Organic Light-Emitting Devices Incorporating a Green Phosphorescence Ultrathin Emitter within a Novel Interface Exciplex for High Efficiency, ACS Appl. Mater. Interfaces. 9 (2017) 10955–10962. https://doi.org/10.1021/acsami.6b16094.

[8] Q. Wang, Q.-S. Tian, Y.-L. Zhang, X. Tang, L.-S. Liao, High-efficiency organic light-emitting diodes with exciplex hosts, J. Mater. Chem. C. 7 (2019) 11329–11360.

https://doi.org/10.1039/C9TC03092A.

[9] R. Zaen, K.M. Park, K.H. Lee, J.Y. Lee, Y. Kang, Blue Phosphorescent Ir(III) Complexes Achieved with Over 30% External Quantum Efficiency, Adv. Opt. Mater. 7 (2019) 1901387. https://doi.org/10.1002/adom.201901387.

[10] H.Y. Park, A. Maheshwaran, C.K. Moon, H. Lee, S.S. Reddy, V.G. Sree, J. Yoon, J.W. Kim, J.H. Kwon, J.J. Kim, S.H. Jin, External Quantum Efficiency Exceeding 24% with CIE_y Value of 0.08 using a Novel Carbene-Based Iridium Complex in Deep-Blue Phosphorescent Organic Light-Emitting Diodes, Adv. Mater. 32 (2020) 2002120. https://doi.org/10.1002/adma.202002120.

[11] X. Gong, J.C. Ostrowski, D. Moses, G.C. Bazan, A.J. Heeger, Electrophosphorescence from a polymer guest-host system with an iridium complex as guest: Förster energy transfer and charge trapping, Adv. Funct. Mater. 13 (2003) 439–444. https://doi.org/10.1002/adfm.200304334.

[12] D. Zhang, M. Cai, Y. Zhang, Z. Bin, D. Zhang, L. Duan, Simultaneous Enhancement of Efficiency and Stability of Phosphorescent OLEDs Based on Efficient Förster Energy Transfer from Interface Exciplex, ACS Appl. Mater. Interfaces. 8 (2016) 3825–3832. https://doi.org/10.1021/acsami.5b10561.

[13] H. Shin, J.-H. Lee, C.-K. Moon, J.-S. Huh, B. Sim, J.-J. Kim, Sky-Blue Phosphorescent OLEDs with 34.1% External Quantum Efficiency Using a Low Refractive Index Electron Transporting Layer, Adv. Mater. 28 (2016) 4920–4925. https://doi.org/10.1002/adma.201506065.

[14] S. Lee, H. Koo, O. Kwon, Y. Jae Park, H. Choi, K. Lee, B. Ahn, Y. Min Park, The Role of Charge Balance and Excited State Levels on Device Performance of Exciplex-based Phosphorescent Organic Light Emitting Diodes, Sci. Rep. 7 (2017) 1–9. https://doi.org/10.1038/s41598-017-12059-2.

[15] Y. Zhang, H. Aziz, Degradation mechanisms in blue phosphorescent organic light-emitting devices by exciton-polaron interactions: Loss in quantum yield versus loss in charge balance, ACS Appl. Mater. Interfaces. 9 (2017) 636–643. https://doi.org/10.1021/acsami.6b13823.

[16] I.R. De Moraes, S. Scholz, B. Lüssem, K. Leo, Analysis of chemical degradation mechanism within sky blue phosphorescent organic light emitting diodes by laser-desorption/ionization time-of-flight mass spectrometry, Org. Electron. 12 (2011) 341–347. https://doi.org/10.1016/j.orgel.2010.11.004.

[17] R. Seifert, I. Rabelo De Moraes, S. Scholz, M.C. Gather, B. Lüssem, K. Leo, Chemical degradation mechanisms of highly efficient blue phosphorescent emitters used for organic light emitting diodes, Org. Electron. 14 (2013) 115–123. https://doi.org/10.1016/j.orgel.2012.10.003.

[18] C. Jeong, C. Coburn, M. Idris, Y. Li, P.I. Djurovich, M.E. Thompson, S.R. Forrest, Understanding molecular fragmentation in blue phosphorescent organic light-emitting devices, Org. Electron. 64 (2019) 15–21. https://doi.org/10.1016/j.orgel.2018.10.001.

[19] Q. Wang, B. Sun, H. Aziz, Exciton-polaron-induced aggregation of wide-bandgap materials and its implication on the electroluminescence stability of phosphorescent organic light-emitting devices, Adv. Funct. Mater. 24 (2014) 2975–2985. https://doi.org/10.1002/adfm.201303840.

[20] A.S.D. Sandanayaka, T. Matsushima, C. Adachi, Degradation Mechanisms of Organic Light-Emitting Diodes Based on Thermally Activated Delayed Fluorescence Molecules, J. Phys. Chem. C. 119 (2015) 23845–23851. https://doi.org/10.1021/acs.jpcc.5b07084.

[21] H. Yu, H. Aziz, Direct Observation of Exciton-Induced Molecular Aggregation in Organic Small-Molecule Electroluminescent Materials, J. Phys. Chem. C. 123 (2019) 16424–16429. https://doi.org/10.1021/acs.jpcc.9b03364.

[22] Y. Zhang, H. Aziz, Influence of the Guest on Aggregation of the Host by Exciton-Polaron Interactions and Its Effects on the Stability of Phosphorescent Organic Light-Emitting Devices, ACS Appl. Mater. Interfaces. 8 (2016) 14088–14095. https://doi.org/10.1021/acsami.6b02946.

[23] M. Penconi, M. Cazzaniga, W. Panzeri, A. Mele, F. Cargnoni, D. Ceresoli, A. Bossi, Unraveling the Degradation Mechanism in FIrpic-Based Blue OLEDs: II. Trap and Detect Molecules at the Interfaces, Chem. Mater. 31 (2019) 2277–2285.

https://doi.org/10.1021/acs.chemmater.8b04502.

[24] C. Yao, Y. Yang, L. Li, M. Bo, C. Peng, J. Wang, Not All Bis[2-(4,6-difluorophenyl)pyridyl-*N, C*2′]iridium(III) Picolinate (FIrpic) Isomers Are Unsuitable for Developing Long-Lifetime Blue Phosphorescent Organic Light-Emitting Diodes, J. Phys. Chem. C. 123 (2019) 227–232. https://doi.org/10.1021/acs.jpcc.8b10599.

[25] Q. Wang, H. Aziz, Exciton-Polaron-Induced Aggregation of Organic Electroluminescent Materials: A Major Degradation Mechanism in Wide-Bandgap Phosphorescent and Fluorescent Organic Light-Emitting Devices, Adv. Opt. Mater. 3 (2015) 967–975. https://doi.org/10.1002/adom.201400640.

[26] S. Kim, H.J. Bae, S. Park, W. Kim, J. Kim, J.S. Kim, Y. Jung, S. Sul, S.G. Ihn, C. Noh, S. Kim, Y. You, Degradation of blue-phosphorescent organic light-emitting devices involves exciton-induced generation of polaron pair within emitting layers, Nat. Commun. 9 (2018) 1211. https://doi.org/10.1038/s41467-018-03602-4.

[27] N.C. Giebink, B.W. D'Andrade, M.S. Weaver, P.B. MacKenzie, J.J. Brown, M.E. Thompson, S.R. Forrest, Intrinsic luminance loss in phosphorescent small-molecule organic light emitting devices due to bimolecular annihilation reactions, J. Appl. Phys. 103 (2008) 044509. https://doi.org/10.1063/1.2884530.

[28] J.-H. Lee, C.-H. Chen, P.-H. Lee, H.-Y. Lin, M. Leung, T.-L. Chiu, C.-F. Lin, Blue organic light-emitting diodes: current status, challenges, and future outlook, J. Mater. Chem. C. 7 (2019) 5874–5888. https://doi.org/10.1039/C9TC00204A.

[29] S. Olthof, R. Meerheim, M. Schober, K. Leo, Energy level alignment at the interfaces in a multilayer organic light-emitting diode structure, Phys. Rev. B. 79 (2009) 245308. https://doi.org/10.1103/PhysRevB.79.245308..

[30] V. Lami, A. Weu, J. Zhang, Y. Chen, Z. Fei, M. Heeney, R.H. Friend, Y. Vaynzof, Visualizing the Vertical Energetic Landscape in Organic Photovoltaics, Joule. 3 (2019) 2513–2534. https://doi.org/10.1016/j.joule.2019.06.018.

[31] S. Lee, H. Ha, J.Y. Lee, H.K. Shon, T.G. Lee, M.C. Suh, Y. Park, Degradation Mechanism of Solution-Processed Organic Light-Emitting Diodes: Sputter Depth-

Profile Study, Appl. Surf. Sci. 564 (2021) 150402. https://doi.org/10.1016/j.apsusc.2021.150402.

[32] H. Aziz, Z. Popovic, C.P. Tripp, N.X. Hu, A.M. Hor, G. Xu, Degradation processes at the cathode/organic interface in organic light emitting devices with Mg:Ag cathodes, Appl. Phys. Lett. 72 (1998) 2642–2644. https://doi.org/10.1063/1.121442.

[33] T. Tong, B. Babatope, S. Admassie, J. Meng, O. Akwogu, W. Akande, W.O. Soboyejo, Adhesion in organic electronic structures, J. Appl. Phys. 106 (2009) 083708. https://doi.org/10.1063/1.3246786.

[34] Q. Wang, Y. Luo, H. Aziz, Evidence of intermolecular species formation with electrical aging in anthracene-based blue organic light-emitting devices, J. Appl. Phys. 107 (2010) 084506. https://doi.org/10.1063/1.3386519.

[35] J.A. McEwan, A.J. Clulow, P.E. Shaw, A. Nelson, T.A. Darwish, P.L. Burn, I.R. Gentle, Diffusion at Interfaces in OLEDs Containing a Doped Phosphorescent Emissive Layer, Adv. Mater. Interfaces. 3 (2016) 1600184. https://doi.org/10.1002/admi.201600184.

[36] J.A. McEwan, A.J. Clulow, A. Nelson, N.R. Yepuri, P.L. Burn, I.R. Gentle, Dependence of Organic Interlayer Diffusion on Glass-Transition Temperature in OLEDs, ACS Appl. Mater. Interfaces. 9 (2017) 14153–14161. https://doi.org/10.1021/acsami.7b01450.

[37] Y.J. Lee, S.-S. Park, J. Kim, H. Kim, Interface morphologies and interlayer diffusions in organic light emitting device by x-ray scattering, Appl. Phys. Lett. 94 (2009) 223305. https://doi.org/10.1063/1.3148648.

[38] J.-R. Gong, L.-J. Wan, S.-B. Lei, C.-L. Bai, X.-H. Zhang, S.-T. Lee, Direct Evidence of Molecular Aggregation and Degradation Mechanism of Organic Light-Emitting Diodes under Joule Heating: an STM and Photoluminescence Study, J. Phys. Chem. B. 109 (2005) 1675–1682. https://doi.org/10.1021/jp046509o.

[39] H.F. Haneef, A.M. Zeidell, O.D. Jurchescu, Charge carrier traps in organic semiconductors: A review on the underlying physics and impact on electronic devices,

J. Mater. Chem. C. 8 (2020) 759–787. https://doi.org/10.1039/c9tc05695e.

[40] S. Olthof, S. Mehraeen, S.K. Mohapatra, S. Barlow, V. Coropceanu, J.-L. Brédas, S.R. Marder, A. Kahn, Ultralow Doping in Organic Semiconductors: Evidence of Trap Filling, Phys. Rev. Lett. 109 (2012) 176601. https://doi.org/10.1103/PhysRevLett.109.176601.

[41] J.-P. Yang, W.-Q. Wang, F. Bussolotti, L.-W. Cheng, Y.-Q. Li, S. Kera, J.-X. Tang, X.-H. Zeng, N. Ueno, Quantitative Fermi level tuning in amorphous organic semiconductor by molecular doping: Toward full understanding of the doping mechanism, Appl. Phys. Lett. 109 (2016) 093302. https://doi.org/10.1063/1.4962052.

[42] M. Oehzelt, K. Akaike, N. Koch, G. Heimel, Energy-level alignment at organic heterointerfaces, Sci. Adv. 10 (2015) e1501127. https://doi.org/10.1126/sciadv.1501127.

[43] J.-P. Yang, F. Bussolotti, S. Kera, N. Ueno, Origin and role of gap states in organic semiconductor studied by UPS: as the nature of organic molecular crystals, J. Phys. D: Appl. Phys. 50 (2017) 423002. https:// doi.org/10.1088/1361-6463/aa840f.

[44] M. Fahlman, S. Fabiano, V. Gueskine, D. Simon, M. Berggren, X. Crispin, Interfaces in organic electronics, Nat. Rev. Mater. 4 (2019) 627–650. https://doi.org/10.1038/s41578-019-0127-y..

[45] S. Duhm, Interface energetics make devices, Electron. Struct. 4 (2022) 034003. https:// doi.org/10.1088/2516-1075/ac884d.